Journal of Quantitative Spectroscopy & Radiative Transfer 112 (2011) 761–768

Contents lists available at ScienceDirect

Journal of Quantitative Spectroscopy & Radiative Transfer

journal homepage: www.elsevier.com/locate/jqsrt

High sensitivity cavity ring down spectroscopy of CO_2 overtone bands near 790 nm

K.-F. Song, Y. Lu, Y. Tan, B. Gao, A.-W. Liu *, S.-M. Hu

Hefei National Laboratory for Physical Sciences at Microscale, University of Science and Technology of China, Hefei 230026, China

ARTICLE INFO

Article history:
Received 29 June 2010
Received in revised form
6 November 2010
Accepted 8 November 2010
Available online 19 November 2010

Keywords:
Carbon dioxide
Vibration–rotation spectroscopy
Cavity ring-down
HITRAN
CDSD

ABSTRACT

The dyad bands of $^{12}C^{16}O_2$ near 790 nm have been recorded with a continuous-wave cavity ring-down spectrometer. Two cold bands and the two associated hot bands are observed in this region. High sensitivity of the 1×10^{-10}/cm level allows one to detect weak transitions with satisfied accuracy. The absolute line intensities have also been retrieved with an estimated accuracy of 2% for majority of the unblended lines. The vibrational transition dipole moment squared values and the empirical Herman–Wallis coefficients are presented for two cold bands. The comparison of the retrieved line positions and intensities with those given in the Carbon Dioxide Spectroscopic Databank shows clear deviation and indicates the empirical calculation can be further improved using the present spectroscopy data.

1. Introduction

As the most important greenhouse gas, the concentration of carbon dioxide in the atmosphere increases by 35% since the beginning of the age of industrialization [1]. Carbon dioxide is a dominant species of the atmosphere of some rocky planets, such as Venus and Mars. Its high-resolution spectroscopy is not only used to monitor the evolution of carbon dioxide in the terrestrial atmosphere for policy makers, but also is an excellent tool for probing atmosphere to different depths. The present work is devoted to the four bands of $^{12}C^{16}O_2$ lying near 12 700 and 13 300 cm^{-1}. One dyad corresponding to the upper state of the hot bands associated to the cold bands are noted as $(10^05)_{1,2}$ and $(11^15)_{1,2}$. The corresponding HITRAN labels of these levels in Fermi resonance are (10051)–(10052) and (11151)–(11152).

The $(10^05)_{1,2}$–$(00^00)_1$ cold bands were first observed by Adams and Dunham in the spectrum of the planet Venus in 1932. In 1953, these Venus bands were recorded with a long multipass cell and several atmospheres in the laboratory by Herzberg and Herzberg [2]. With the development of high sensitivity laser spectroscopy techniques, the $(10^05)_{1,2}$–$(00^00)_1$ bands were studied by photo acoustic (PA) [3], intra-cavity laser absorption spectroscopy (ICLAS) [4] and tunable diode laser spectroscopy (TDLs) [5,6]. Because of the large Doppler broadening and/or the lack of accurate reference standards in the region over 12 500 cm^{-1}, the accuracy of ro-vibrational parameters for these vibrational states is limited. As a result, the HITRAN08 database [8] data corresponding to Venus bands above 9650 cm^{-1} were taken from the CDSD databank [7].

Here we present the cavity ring-down spectroscopy (CRDS) of natural carbon dioxide sample near the 0.8 μm region. Superior sensitivity and resolution allow us to observe the weak bands with much better accuracy.

The present paper is organized as follows. In Section 2, the experimental procedure and the methodology of the analysis are presented. Section 3 is devoted to the band-by-band analysis and the modeling of the spectral parameters. Some discussions and conclusions are given in Section 4.

2. Experiment and data reduction

A continuous-wave (CW) CRDS spectrometer has been developed using a CW tunable Ti-sapphire laser over the

* Corresponding author. Fax: +86 551 3607632.
E-mail address: awliu@ustc.edu.cn (A.-W. Liu).

0022-4073/$ - see front matter © 2010 Elsevier Ltd. All rights reserved.
doi:10.1016/j.jqsrt.2010.11.006

spectral range of 780–830 nm. The details of the cavity ring-down spectrometer are presented in Refs. [9,10]. In brief, the structure of the setup is as follows: A CW tunable Ti:sapphire laser (Coherent 899-21) beam is carefully coupled into a 1.2 m long resonance cavity. The cavity mirrors (Los Gatos Inc.) have a reflectivity of 99.995% and one of the two mirrors is mounted on a piezoelectric actuator (PI Inc.). The piezoelectric actuator is driven with a triangle wave from a function generator. The Ti:Sa laser is running in a step-scan mode controlled by a personal computer (PC). On each step, typically about 100 ring-down events are recorded with a fast digitizer (ADLINK PCI-9820). The digitizer is working at a sampling rate of 1 MS/s (mega-samples per second) with 14-bit resolution. A fitting

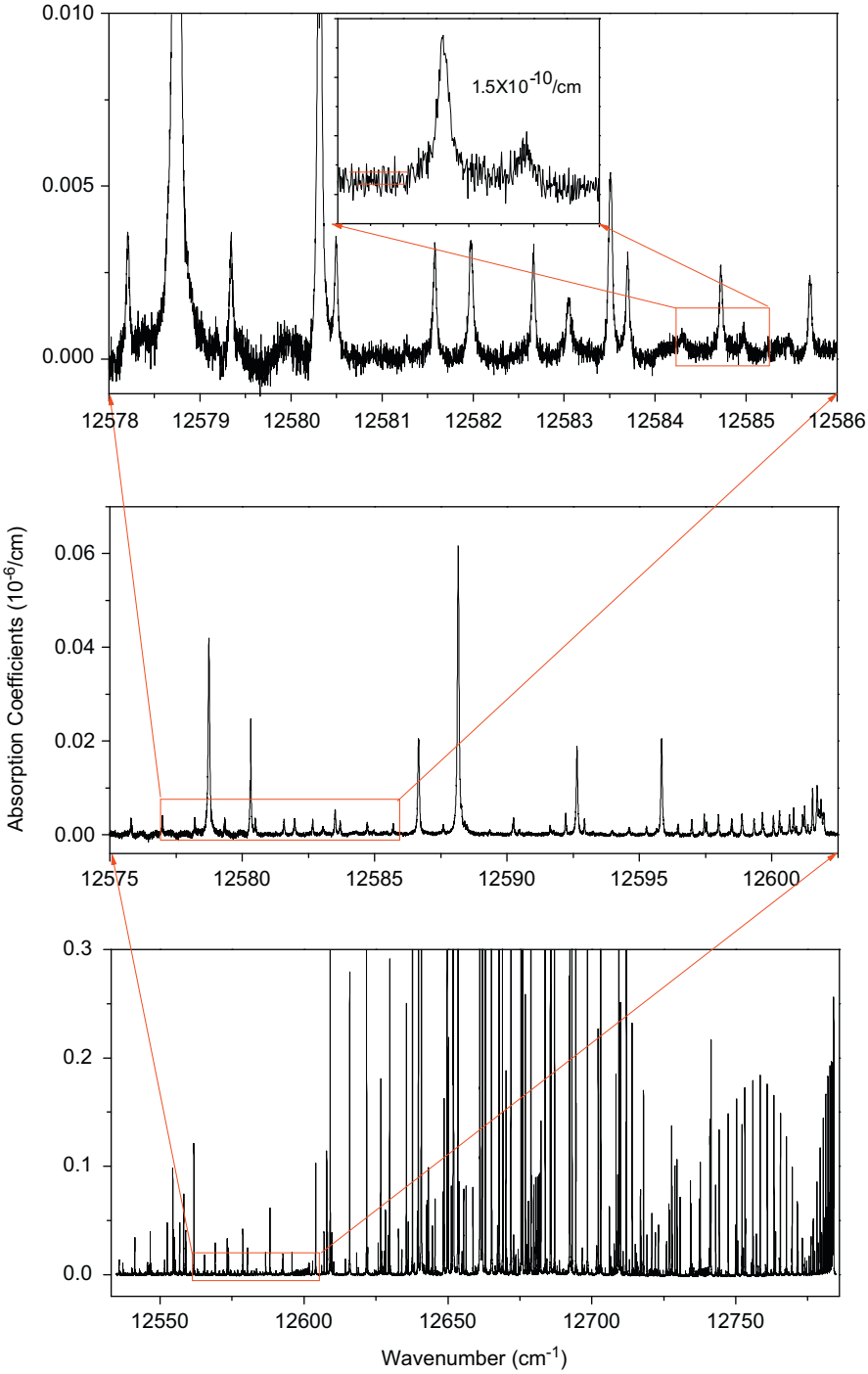

Fig. 1. Overview of the CRDS spectrum of carbon dioxide around 790 nm. Sample pressure: 103.3 Torr. Three successive enlargements illustrate the achieved signal to noise ratio. The insert shows the noise equivalent absorption of about 1.5×10^{-10}/cm.

program which follows the method proposed by Halmer et al. [11] is applied to fit the exponentially decay curve and to give the decay time τ. The sample absorption coefficient, α, can be derived from

$$\alpha = \frac{1}{c}\left(\frac{1}{\tau} - \frac{1}{\tau_0}\right) \quad (1)$$

where c is the speed of light, τ and τ_0 are the decay time of the cavity with and without sample, respectively.

Natural CO_2 gas sample was filled into the resonance cavity at room temperature. The sample pressure was 103.3 Torr measured with a capacitance manometer (MKS Baratron 627B) with an accuracy of 0.15%. The spectrum calibration is based on the readings given by a λ−meter (Burleigh WA1500) and has been described in details in Ref. [10]. It is checked and refined by using some reference lines for the whole region. The water line positions were taken from Ref. [12]. An overview of the CW-CRDS spectra is presented in Fig. 1, and three successive enlargements illustrate the quality of spectrum and good signal to noise ratio. The noise equivalent minimum detectable absorption loss is estimated to be 1.5×10^{-10}/cm.

3. Results

3.1. Transition list

A total of four bands of $^{12}C^{16}O_2$ were detected near 790 nm. The line parameters of each observed line were retrieved using an interactive least squares multi-lines fitting procedure. Since the instrumental linewidth was estimated less than 1×10^{-4} cm^{-1} [10] and is much smaller than the Doppler broadening, the instrumental profile was neglected in the fitting. A Voigt line profile was adopted and the Gaussian component width was fixed to the calculated Doppler width. Line position, integrated line absorbance, Lorentzian width of each line and a baseline were given by the fitting procedure ("Intwin" [13]). The position uncertainty of unblended and not-very-weak lines is estimated to be 0.001 cm^{-1}. The main error on the line strength values comes from the line profile fitting, especially uncertainty on the baseline. The fitting error is estimated to be around 0.6% for well-isolated and unblended lines. Including the pressure uncertainty (0.15%) and the error from the temperature fluctuation ($<1\%$), the accuracy of the line intensities is estimated to

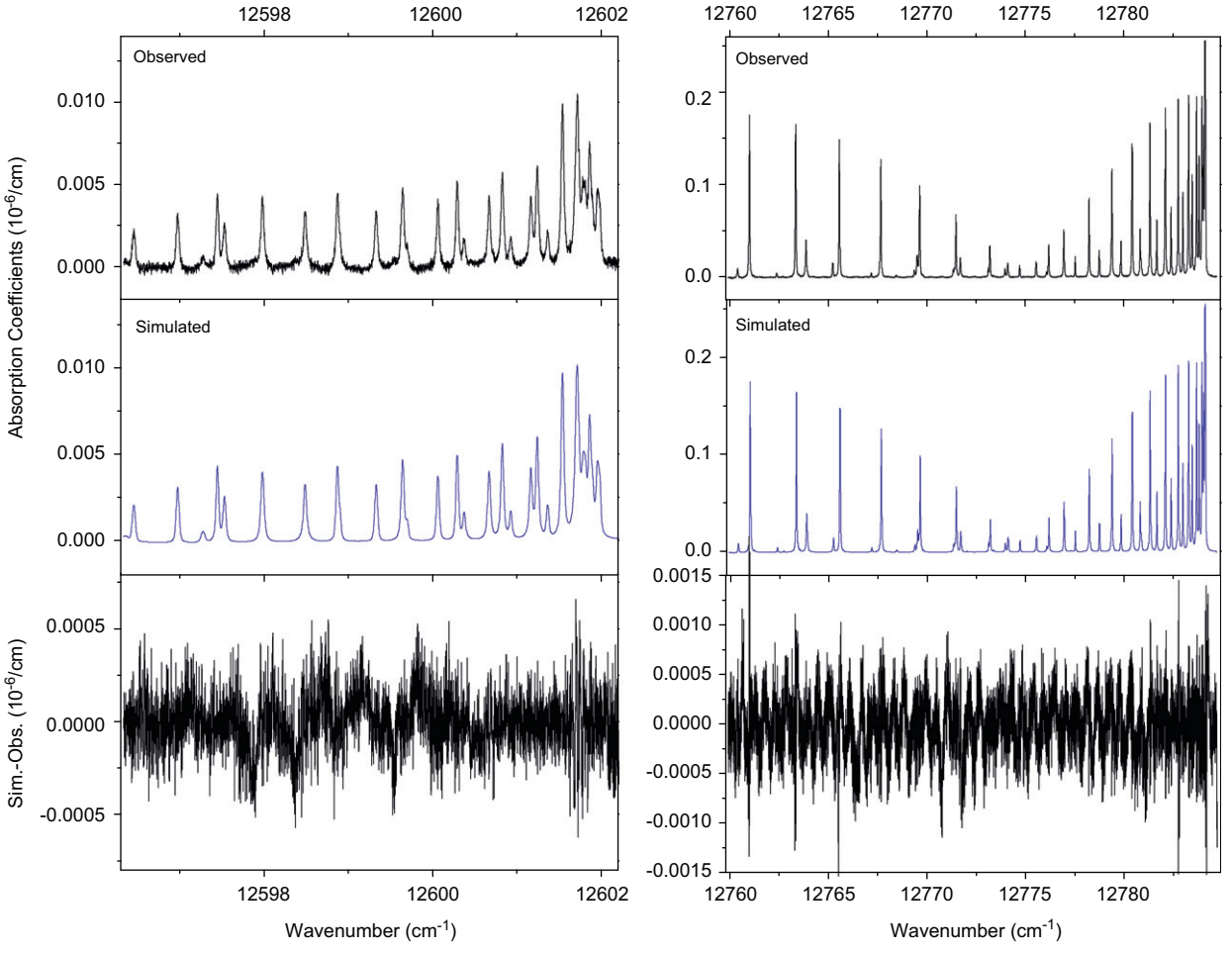

Fig. 2. Part of the observed CRDS spectrum (upper), simulated spectrum (middle) obtained as a sum of individual Voigt profiles, and the residuals (lower). Note that the weak lines in the left panels are about three orders of magnitude weaker than the strong lines in the right panels.

Table 1
Line parameters of the $(10^05)_1$–$(00^00)_1$ band of $^{12}C^{16}O_2$.

Line	Position	S_{obs}	S_{cal}	%	$\lvert R\rvert^2_{obs}$
P 56	12683.0584*	2.58E−29	4.03E−29	−56.0	1.06E−11
P 54	12687.9967*	1.43E−28	5.94E−29	58.4	3.98E−11
P 52	12692.8145*	6.18E−29	8.61E−29	−39.2	1.19E−11
P 50	12697.5105	1.31E−28	1.23E−28	6.1	1.78E−11
P 48	12702.0833*	1.28E−28	1.72E−28	−34.4	1.25E−11
P 46	12706.5366*	2.57E−28	2.37E−28	7.6	1.82E−11
P 44	12710.8639	3.20E−28	3.21E−28	−0.3	1.68E−11
P 42	12715.0700	4.28E−28	4.28E−28	−0.1	1.69E−11
P 40	12719.1539	5.84E−28	5.60E−28	4.1	1.77E−11
P 38	12723.1134	7.18E−28	7.20E−28	−0.3	1.70E−11
P 36	12726.9496	9.09E−28	9.09E−28	0.0	1.70E−11
P 34	12730.6613	1.17E−27	1.13E−27	3.3	1.77E−11
P 32	12734.2508	1.37E−27	1.37E−27	0.1	1.71E−11
P 30	12737.7149	1.65E−27	1.64E−27	0.8	1.73E−11
P 28	12741.0550	2.00E−27	1.91E−27	4.1	1.79E−11
P 26	12744.2723	2.21E−27	2.19E−27	0.7	1.74E−11
P 24	12747.3632	2.48E−27	2.46E−27	0.7	1.74E−11
P 22	12750.3311	2.70E−27	2.70E−27	−0.1	1.73E−11
P 20	12753.1743	2.90E−27	2.90E−27	0.0	1.73E−11
P 18	12755.8914	3.06E−27	3.03E−27	1.0	1.75E−11
P 16	12758.4852	3.23E−27	3.08E−27	4.5	1.82E−11
P 14	12760.9533	3.03E−27	3.04E−27	−0.2	1.74E−11
P 12	12763.2977	2.89E−27	2.89E−27	0.2	1.75E−11
P 10	12765.5146	2.64E−27	2.63E−27	0.5	1.75E−11
P 8	12767.6089	2.14E−27	2.26E−27	−5.6	1.65E−11
P 6	12769.5763	1.81E−27	1.80E−27	0.6	1.76E−11
R 52	12771.3400	8.72E−29	8.98E−29	−3.0	1.64E−11
P 4	12771.4200	1.24E−27	1.25E−27	−1.2	1.73E−11
R 50	12773.0533	1.29E−28	1.28E−28	1.1	1.72E−11
P 2	12773.1374	6.20E−28	6.43E−28	−3.7	1.69E−11
R 48	12774.6433	1.78E−28	1.80E−28	−0.7	1.69E−11
R 0	12775.4777	3.22E−28	3.25E−28	−1.0	1.73E−11
R 2	12776.8842	9.43E−28	9.65E−28	−2.4	1.71E−11
R 44	12777.4545	3.17E−28	3.35E−28	−5.7	1.62E−11
R 4	12778.1618	1.58E−27	1.57E−27	0.8	1.77E−11
R 42	12778.6745	4.43E−28	4.47E−28	−0.8	1.70E−11
R 6	12779.3155	2.11E−27	2.10E−27	0.1	1.75E−11
R 40	12779.7708	6.07E−28	5.85E−28	3.7	1.78E−11
R 8	12780.3426	2.55E−27	2.56E−27	−0.0	1.75E−11
R 38	12780.7422	7.47E−28	7.52E−28	−0.7	1.71E−11
R 10	12781.2457	2.91E−27	2.91E−27	0.2	1.75E−11
R 36	12781.5900	9.66E−28	9.50E−28	1.7	1.75E−11
R 12	12782.0239	3.15E−27	3.15E−27	0.0	1.75E−11
R 34	12782.3122	1.18E−27	1.18E−27	0.2	1.73E−11
R 14	12782.6755	3.32E−27	3.27E−27	1.5	1.78E−11
R 32	12782.9117	1.41E−27	1.43E−27	−1.8	1.70E−11
R 16	12783.2012	3.32E−27	3.30E−27	0.8	1.76E−11
R 30	12783.3840	1.72E−27	1.71E−27	0.1	1.74E−11
R 18	12783.6037	3.24E−27	3.23E−27	0.4	1.75E−11
R 28	12783.7338	2.04E−27	2.01E−27	1.3	1.76E−11
R 20	12783.8796	3.05E−27	3.07E−27	−0.6	1.73E−11
R 26	12783.9571*	2.41E−27	2.31E−27	4.2	1.82E−11
R 22	12784.0290*	3.12E−27	2.86E−27	8.4	1.90E−11
R 24	12784.0534*	2.13E−27	2.59E−27	−22.0	1.43E−11

*: Blended lines.

Table 2
Line parameters of the $(10^05)_2$–$(00^00)_1$ band of $^{12}C^{16}O_2$.

Line	Position	S_{obs}	S_{cal}	%	$\lvert R\rvert^2_{obs}$
P 52	12592.9242	4.68E−29	4.70E−29	−0.4	9.11E−12
P 50	12597.4490	6.47E−29	6.60E−29	−2.0	8.87E−12
P 48	12601.8557	9.24E−29	9.13E−29	1.1	9.06E−12
P 46	12606.1380	1.28E−28	1.24E−28	3.3	9.17E−12
P 44	12610.3045	1.74E−28	1.66E−28	4.5	9.20E−12
P 42	12614.3578	2.18E−28	2.19E−28	−0.3	8.68E−12
P 40	12618.2869	2.79E−28	2.83E−28	−1.5	8.50E−12
P 38	12622.0995	3.49E−28	3.59E−28	−2.9	8.31E−12
P 36	12625.7986	4.45E−28	4.49E−28	−0.9	8.41E−12
P 34	12629.3751	5.65E−28	5.51E−28	2.5	8.63E−12
P 32	12632.8346	6.57E−28	6.64E−28	−1.0	8.28E−12
P 30	12636.1767	7.69E−28	7.85E−28	−2.1	8.13E−12
P 28	12639.4014	9.12E−28	9.11E−28	0.2	8.27E−12
P 26	12642.5097	1.05E−27	1.04E−27	1.4	8.32E−12
P 24	12645.5021	1.12E−27	1.15E−27	−3.4	7.89E−12
P 20	12651.1316*	1.27E−27	1.34E−27	−5.8	7.63E−12
P 18	12653.7721	1.37E−27	1.39E−27	−1.6	7.92E−12
P 16	12656.2953	1.36E−27	1.41E−27	−3.3	7.76E−12
P 14	12658.7015	1.41E−27	1.38E−27	1.8	8.13E−12
P 10	12663.1648	1.20E−27	1.19E−27	1.3	8.05E−12
P 6	12667.1618	7.70E−28	8.08E−28	−5.0	7.54E−12
P 2	12670.6908*	3.15E−28	2.88E−28	8.5	8.64E−12
R 0	12673.0331*	1.58E−28	1.46E−28	7.9	8.58E−12
R 50	12673.1670*	5.53E−29	6.81E−29	−23.2	7.38E−12
R 2	12674.4478	4.29E−28	4.32E−28	−0.7	7.85E−12
R 48	12674.5840*	1.19E−28	9.43E−29	20.5	1.13E−11
R 4	12675.7469	6.68E−28	7.02E−28	−5.1	7.53E−12
R 44	12677.0600*	1.85E−28	1.72E−28	7.2	9.51E−12
R 8	12677.9922	1.18E−27	1.15E−27	2.7	8.16E−12
R 42	12678.1191	2.20E−28	2.26E−28	−2.9	8.50E−12
R 10	12678.9400	1.26E−27	1.31E−27	−4.1	7.64E−12
R 40	12679.0563*	2.72E−28	2.93E−28	−7.4	8.07E−12
R 12	12679.7730	1.42E−27	1.42E−27	−0.2	7.96E−12
R 38	12679.8782	3.61E−28	3.72E−28	−3.2	8.33E−12
R 14	12680.4855	1.43E−27	1.49E−27	−3.8	7.71E−12
R 36	12680.5779	4.63E−28	4.65E−28	−0.6	8.47E−12
R 16	12681.0822	1.55E−27	1.50E−27	2.9	8.27E−12
R 34	12681.1608*	5.40E−28	5.72E−28	−5.8	7.99E−12
R 18	12681.5619	1.53E−27	1.48E−27	3.6	8.37E−12
R 32	12681.6247*	7.39E−28	6.90E−28	6.6	8.99E−12
R 20	12681.9232	1.43E−27	1.41E−27	1.0	8.18E−12
R 30	12681.9681	8.42E−28	8.17E−28	3.0	8.59E−12
R 22	12682.1687	1.31E−27	1.32E−27	−1.3	8.03E−12
R 28	12682.1957*	1.13E−27	9.50E−28	16.2	9.88E−12
R 24	12682.2989*	2.22E−27	1.21E−27	45.6	1.50E−11

*: Blended lines.

be 2% or less for a majority of the lines. For those blended lines, the error may reach 10% since the baseline uncertainty is supposed to be much larger (Fig. 2).

A total of 209 $^{12}C^{16}O_2$ line transitions was observed. The full line list is presented in Tables 1–3. The line strength values in the tables have been converted to the one with 98.42% as adopted in HITRAN and temperature at 296 K.

3.2. Spectroscopic constants of the upper states

Four vibrational transitions were rotationally identified with the help of CDSD calculations. The standard expression for the vibration–rotation energy levels was used to determine the spectroscopic parameters:

$$F_v(J) = G_v + B_vJ(J+1) - D_vJ^2(J+1)^2 + H_vJ^3(J+1)^3 \quad (2)$$

In Eq. (2), G_v is the vibrational term value, B_v is the rotational constant, D_v and H_v are the centrifugal distortion constants. The spectroscopic parameters for an upper state were fitted directly to the observed line positions of the respective band, and in the case of hot bands involving *e* and *f* components, the *ee* and *ff* sub bands were considered separately. The lower state rotational constants were constrained to their literature values [14] in the fitting.

Table 3
Experimental line list of the $(11^15)_1$–$(01^10)_1$ and $(11^15)_2$–$(01^10)_1$ bands of $^{12}C^{16}O_2$.

$(11^15)_1$–$(01^1\,0)_1$						$(11^15)_2$- $(01^10)_1$					
e–e			f–f			e–e			f–f		
Line	Position	S_{obs}	Line	Position	S_{obs}	Line	Position	S_{obs}	Line	Position	S_{obs}
P 45	12666.1326	1.36E−29	P 46	12664.0851	6.37E−29	P 37	12543.3148	1.17E−29	P 4	12588.4883	3.58E−29
P 35	12686.1202	3.43E−29	P 44	12668.3688	5.87E−30	P 35	12546.9619	1.29E−29	P 12	12580.4955	5.37E−29
P 33	12689.7533	8.82E−29	P 42	12672.5387	1.33E−29	P 33	12550.4989	3.18E−29	P 22	12567.9047	4.63E−29
P 27	12699.9100	9.92E−29	P 40	12676.5917	2.43E−29	P 31	12553.9097	4.28E−29	P 24	12565.0394	3.47E−29
P 19	12711.7223	1.08E−28	P 32	12691.5600	3.86E−29	P 29	12557.2064	4.16E−29	P 26	12562.0579	5.12E−29
P 17	12714.3680	9.45E−29	P 30	12694.9998	5.26E−29	P 27	12560.3839	4.43E−29	R 4	12595.2673	3.46E−29
P 13	12719.2879	8.62E−29	P 26	12701.5097	6.92E−29	P 25	12563.4461	2.90E−29	P 8	12584.7232	5.09E−29
P 11	12721.5622	8.04E−29	P 24	12704.5818	8.23E−29	P 23	12566.3886	6.28E−29	P 20	12570.6523	7.12E−29
P 9	12723.7132	7.52E−29	P 22	12707.5325	1.03E−28	P 19	12571.9186	8.21E−29	R 8	12597.5322	4.22E−29
P 7	12725.7397	6.73E−29	P 20	12710.3600	1.05E−28	P 17	12574.5126	7.57E−29	P 14	12578.2075	5.40E−29
P 3	12729.4259	4.49E−29	P 16	12715.6439	9.69E−29	P 15	12576.9854	6.92E−29	R 10	12598.4873	6.83E−29
R 1	12733.3243	2.06E−29	P 14	12718.1020	1.15E−28	P 13	12579.3425	4.98E−29	P 30	12555.7527	4.00E−29
R 3	12734.6778	4.03E−29	P 12	12720.4376	9.20E−29	P 11	12581.5796	5.25E−29	R 40	12598.9027	1.38E−29
R 43	12735.5764	1.45E−29	P 10	12722.6488	7.64E−29	P 9	12583.6979	4.73E−29	R 12	12599.3290	5.31E−29
R 5	12735.8990	9.31E−29	P 8	12724.7379	7.95E−29	P 7	12585.7025	3.79E−29	R 6	12596.4585	3.58E−29
R 41	12736.7030	1.32E−29	P 4	12728.5445	2.76E−29	P 5	12587.5885	3.94E−29	R 38	12599.6986	8.91E−30
R 7	12736.9958	9.49E−29	P 2	12730.2645	1.27E−29	P 3	12589.3511	1.09E−29	R 14	12600.0600	5.89E−29
R 9	12737.9706	9.37E−29	R 2	12734.0243	2.52E−29	R 1	12593.2495	9.09E−30	R 2	12593.9668	1.73E−29
R 37	12738.5911	3.47E−29	R 44	12735.1900	1.14E−29	R 3	12594.6137	4.39E−29	R 36	12600.3717	2.92E−29
R 11	12738.8175	1.06E−28	R 42	12736.3654	3.24E−29	R 7	12596.9782	4.94E−29	R 16	12600.6662	7.17E−29
R 35	12739.3492	3.53E−29	R 6	12736.4752	9.91E−29	R 9	12597.9827	7.86E−29	P 34	12548.9776	8.24E−29
R 13	12739.5447	1.10E−28	R 8	12737.5165	6.67E−29	R 11	12598.8696	6.55E−29	R 34	12600.9228	2.54E−29
R 33	12739.9862	2.54E−29	R 10	12738.4331	8.98E−29	R 13	12599.6423	8.83E−29	R 18	12601.1604	7.05E−29
R 15	12740.1456	1.12E−28	R 36	12739.1445	4.69E−29	R 15	12600.2888	7.38E−29	P 10	12582.6629	4.98E−29
R 31	12740.4977	4.04E−29	R 12	12739.2268	1.28E−28	R 17	12600.8225	9.39E−29	R 32	12601.3597	2.63E−29
R 17	12740.6231	1.06E−28	R 34	12739.8281	5.06E−29	R 19	12601.2364	9.61E−29	P 36	12545.4138	1.23E−29
R 27	12741.1551	3.08E−28	R 14	12739.8977	1.12E−28	R 21	12601.5357	1.61E−28	P 16	12575.8027	5.56E−29
			R 32	12740.3872	5.08E−29						
			R 16	12740.4443	1.22E−28						

The spectroscopic parameters retrieved from the fitting are presented in Table 4. The *rms* value of the (obs.-calc.) deviations are generally 1×10^{-3} cm^{-1} which is consistent with the experimental accuracy. The corresponding spectroscopic parameters reported in the literature are also reviewed in italics and included in Table 4.

3.3. Vibrational transition dipole moment squared, and Herman–Wallis factor

The line intensity $S(T_0)$ in cm^{-1}/(cm^{-2} mol) at the standard temperature T_0=296 K can be deduced using the following equation:

$$S(T_0)=\frac{1}{4\pi\varepsilon_0}\frac{8\pi^3\nu_0}{3hcQ(T_0)}|R|^2L(J,\ell)e^{-hcE''/kT_0}[1-e^{-hc\nu_0/kT_0}] \quad (3)$$

In Eq. (3), $1/4\pi\varepsilon_0=10^{-36}$ erg cm^3 D^{-2}; h is Planck's constant; c is the vacuum speed of light; ν_0 is the transition wavenumber in cm^{-1}; $Q(T_0)$ is the total partition function at temperature T_0; $L(J,\ell)$ is the Hönl–London factor; J is the lower state rotational quantum number; ℓ is the quantum number of the projection of the vibrational angular momentum on the molecular axis; E'', in cm^{-1} is the lower level energy; and k is the Boltzmann constant.

For those two parallel bands, the Hönl–London factor $L(J,\ell)$ is equal to $|m|$, where m is $-J$ for P branch, and $J+1$ for R branch. For the isolated vibrational states of a linear molecule, the rotational dependence of the transition dipole moment squared can be expressed with

$$|R|^2=|R_0|^2F(m) \quad (4)$$

where $|R|^2$ is the vibrational transition dipole moment squared, $F(m)$ is the empirical Herman–Wallis factor which can be interpreted with

$$F(m)=(1+A_1m+A_2m^2)^2 \quad (5)$$

where A_1 and A_2 are the Herman–Wallis coefficients. In this case, the vibrational transition dipole moment squared and the Herman–Wallis coefficients are retrieved from the fitting of the line intensities corresponding to unblended transitions, and they are given in Table 4. The line intensities calculated with this set of Herman–Wallis coefficients are given in Tables 1 and 2 for the $(10^05)_{1,2}$–$(00^00)_1$ cold bands. The blended lines marked with "*" in the tables were excluded from the fit. In Fig. 3, the plot of the transition dipole moment squared versus rotational quantum number m is given for two cold bands in the upper and lower panels, respectively.

4. Discussion and conclusion

Significant progress on the carbon dioxide spectroscopy data has been made in the latest HITRAN [8] database owing to the Fourier transform spectroscopy measurements carried out in the Jet Propulsion Laboratory [15], CRDS observations in the 5851–7045 cm^{-1} region from Laboratoire de Spectrométrie

Table 4
Spectroscopic constants (in cm^{-1}), vibrational transition moments $|R_v|^2$ (in D^2; D, Debye), Herman–Wallis parameters of the $^{12}C^{16}O_2$ bands observed in the present study.

States	G_v			B_v			$D_v \times 10^7$		
Lower states constants									
$(00^00)_1e$	0.00000			0.39021894			1.334088		
$(01^10)_1e$	667.3798265			0.390639109			1.35393		
$(01^10)_1f$	667.3798265			0.391254698			1.361606		
Band	ΔG_v[a]	B_v	$D_v \times 10^7$	J_{MAX} P/R	n/N[b]	RMS[c]	$\|R\|^2 \times 10^{11}$	$A_1 \times 10^5$	$A_2 \times 10^5$
$(10^05)_2e$–$(00^00)_1e$	12672.28163(24)	0.37563636(53)	1.5828(21)	52/50	40/45	0.76	0.7901(78)	0.0[d]	2.81(41)
JMS1999[e]	*12672.2833(1)*	*0.37563425(9)*	*1.5695(3)*						
$(10^05)_1e$–$(00^00)_1e$	12774.72961(17)	0.37454991(35)	1.1249(13)	56/52	52/54	0.66	1.7503(52)	9.1(40)	−0.77(14)
JMS1999[e]	*12774.7310(1)*	*0.3745506(2)*	*1.1264(5)*						
$(11^15)_2e$–$(01^10)_1e$	12591.78750(59)	0.3759524(26)	1.527(20)	37/21	22/27	1.22			
$(11^15)_2f$–$(01^10)_1f$	12591.79144(68)	0.3768050(29)	1.514(19)	36/40	20/27	1.41			
$(11^15)_1e$–$(01^10)_1e$	12731.86183(35)	0.3751385(13)	1.1626(71)	45/43	22/27	0.89			
$(11^15)_1f$–$(01^10)_1f$	12731.86135(25)	0.37583391(81)	1.1569(41)	46/44	25/29	0.70			

Note: The lower state constants were fixed at the values of Ref. [14]. The uncertainties are given in parenthesis in the unit of the last quoted digit.
[a] Difference between the upper and lower vibrational term values.
[b] *n*: number of transitions included in the fit; *N*: number of assigned rotational transitions.
[c] Root mean square deviation (in 10^{-3} cm^{-1}).
[d] Values were fixed to zero.
[e] Values from Ref. [17].

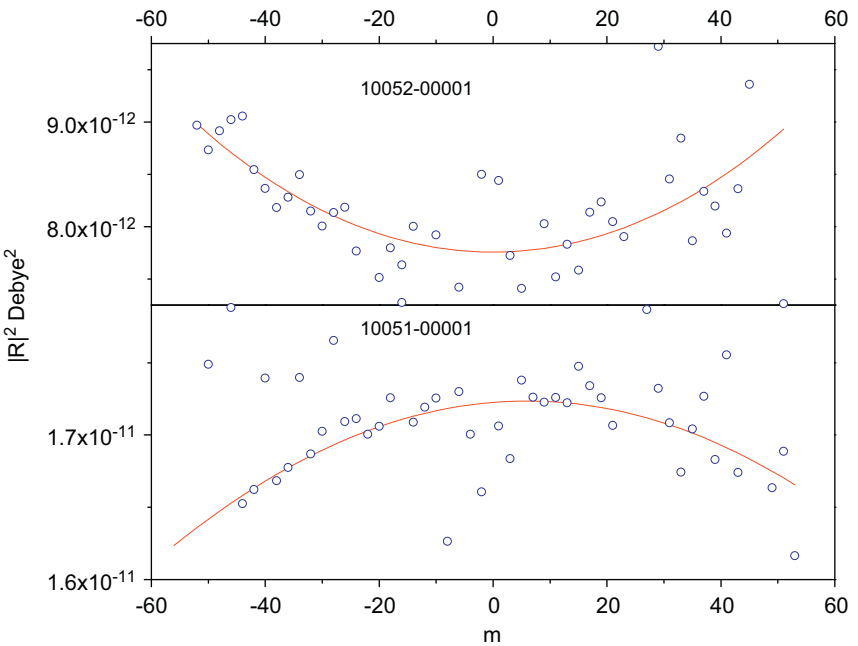

Fig. 3. Experimental (open circles) and calculated (solid lines) values of the transitions dipole moment squared of the $(10^05)_{1,2}$ cold bands of carbon dioxide. The calculated $|R|^2$ values were obtained using the parameters given in Table 4.

Physique, UJF, Grenoble [16], and the high quality theoretical calculation (CDSD). All lines above 9650 cm^{-1} given in HITRAN08 are actually calculated results from CDSD, including those four bands recorded in present measurement. Although as mentioned in the introduction part, the $(10^05)_{1,2}$–$(00^00)_1$ bands have been studied with FTS, PA, ICLAS and TDLs before. The stated accuracy of the ro-vibrational energy levels of the $(10^05)_{1,2}$ state reaches 1×10^{-4} cm^{-1} with the $(10^05)_{1,2}$–$(10^04)_{1,2}$ FT emission spectra near 4.5 μm provided by Campargue et al. and verified by the *Ritz* principle [17]. However, the line position accuracy of TDLs is only within 0.01 cm^{-1}. Therefore, on the one hand, we compared our

results with the CDSD calculations, on the other hand, the line positions of the $(10^05)_{1,2}$–$(00^00)_1$ bands were also compared with the experimental values determined by *Ritz* principle calculations [17].

Fig. 4 shows the line position deviations of the observations from HITRAN08 values and *Ritz* ones in the upper and lower panels, respectively. For previously reported $(10^05)_{1,2}$–$(00^00)_1$ cold bands, it is obvious that the *Ritz* values agrees well with the line positions from present CW-CRDS measurement. However, the HITRAN08 values have systematic shifts of about 0.005 and 0.002 cm^{-1} for the dyads, respectively. The largest deviation (HITRAN-obs.) is

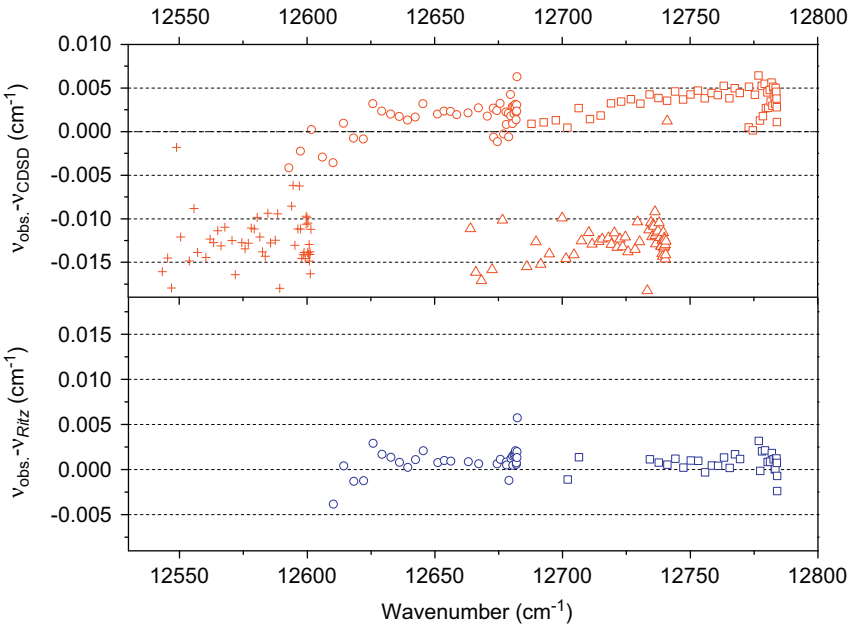

Fig. 4. Comparison of the experimental $^{12}C^{16}O_2$ line positions and those given in HITRAN2008 database [8] (upper panel) and those from Ritz retrieval [17] (lower panel). Square: $(10^05)_1$–$(00^00)_1$; circle: $(10^05)_2$–$(00^00)_1$; triangle: $(11^15)_1$–$(01^10)_1$; cross: $(11^15)_2$–$(01^10)_1$.

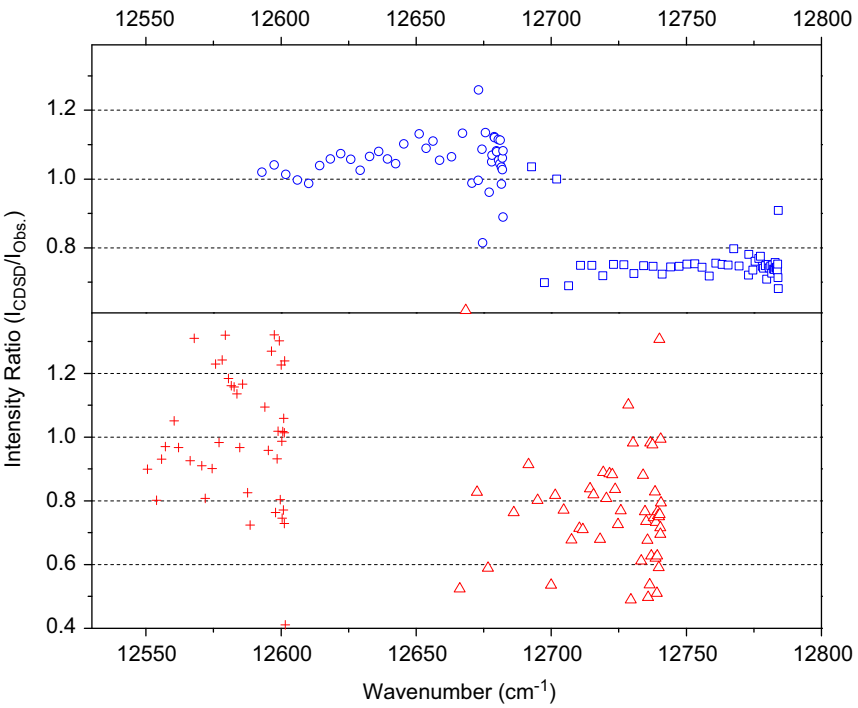

Fig. 5. Comparison of the experimental $^{12}C^{16}O_2$ line intensities and the CDSD calculations. Upper panel: the $(10^05)_{1,2}$–$(00^00)_1$ cold bands. Lower panel: the $(11^15)_{1,2}$–$(01^10)_1$ hot bands.

$-0.026\ cm^{-1}$ for the $R(1)$ line of e–e branch of the $(11^15)_2$–$(01^10)_1$ band. The mean deviation for both hot bands is about $-0.015\ cm^{-1}$. Such deviation is consistent with the average residual of the CDSD calculations.

The agreement of line intensities between different databases is another criterion to verify the present experimental accuracy. Now, there are three experimental intensities: ICLAS, TDLs and CRDS. Due to the principle of 2*f* spectrum, the TDLs intensities are not reliable and reproducible. The line intensities given in Refs. [5,6] are 20 times the CDSD calculations on average. So only comparisons of the intensity values between the present work and the CDSD calculations are presented for cold and hot bands in the upper and lower panels of Fig. 5, respectively. In fact, the $(10^05)_{1,2}$–$(00^00)_1$ band intensities have been measured with ICLAS technique by Campargue et al. [4]. Although ICLAS is also very sensitive, due to the overlapped atmospheric water absorption in the 760–850 nm region, the uncertainties of the absolute intensities from ICLAS often exceed 20%. It is clear that the overall agreement is satisfactory for the $(10^05)_2$–$(00^00)_1$ and $(11^15)_2$–$(01^10)_1$ bands. As for the $(10^05)_1$–$(00^00)_1$ and $(11^15)_1$–$(01^10)_1$ bands, the CDSD calculations are underestimated by 20%. No doubt that the present new experimental results will help for further improvement of the databases and other applications like the studies of the Venus atmosphere [18].

Acknowledgments

This work is jointly supported by NSFC-China (Grant nos. 20903085, 20873132, 10728408), and by Chinese Ministry of Science and Technology (2007CB815203).

References

[1] After two large annual gains, rate of atmospheric CO_2 increase returns to average. NOAA News Online, Story 2412. 2005-03-31.

[2] Herzberg G, Herzberg L. Rotation–vibration spectra of diatomic and simple polyatomic molecules with long absorbing paths. J Opt Soc Am 1953;43:1037–44.

[3] Yang XK, Petrillo CJ, Noda C. Photoacoustic detection of N_2O and CO_2 overtone transitions in the near-infrared. Chem Phys Lett 1993;214:536–40.

[4] Campargue A, Charvat A, Permogorov D. Absolute intensity measurement of CO_2 overtone transitions in the near-infrared. Chem Phys Lett 1994;223:567–72.

[5] Lucchesini A, Gozzini S. Diode laser overtone spectroscopy of CO_2 at 780 nm. J Quant Spectrosc Radiat Transfer 2005;96:289–99.

[6] Lucchesini A, Gozzini S. Diode laser spectroscopy of CO_2 at 790 nm. J Quant Spectrosc Radiat Transfer 2007;103:74–82.

[7] Perevalov VI, Tashkun SA. CDSD-296 (Carbon Dioxide Spectroscopic Databank): updated and enlarged version for atmospheric applications. In: 10th HITRAN database conference. Cambridge, MA, USA, 2008.

[8] Rothman LS, Gordon IE, Barbe A, Chris Benner D, Bernath PF, Birk M, et al. The HITRAN 2008 molecular spectroscopic database. J Quant Spectrosc Radiat Transfer 2009;110:533–72.

[9] Gao B, Liu AW, Wu RX, Ning W, Hu SM. C_2H_2 overtones near $12\,300\ cm^{-1}$ revisited with a very sensitive cavity ring-down spectrometer. Chin J Chem Phys 2009;22:663–7.

[10] Gao B, Jiang W, Liu AW, Lu Y, Cheng CF, Cheng GS, et al. Ultra sensitive near-infrared cavity ring down spectrometer for precise line profile measurement. Rev Sci Instrum 2010;81:043105.

[11] Halmer D, Basum GV, Hering P, Müartz M. Fast exponential fitting algorithm for real-time instrumental use. Rev Sci Instrum 2004;75:2187–91.

[12] Tolchenov R, Tennyson J. Water line parameters from refitted spectra constrained by empirical upper state levels: study of the 9500–$14\,500\ cm^{-1}$ region. J Quant Spectrosc Radiat Transfer 2008;109:559–68.

[13] Wang L, Perevalov VI, Tashkun SA, Gao B, Hao LY, Hu SM. Fourier transform spectroscopy of N_2O weak overtone transitions in the 1−2 μm region. J Mol Spectrosc 2006;237:129–36.

[14] Miller CE, Brown LR. Near infrared spectroscopy of carbon dioxide I. $^{16}O^{12}C^{16}O$ line positions. J Mol Spectrosc 2004;228:329–54.

[15] Toth RA, Brown LR, Miller CE, Devi VM, Benner DC. Line strengths of $^{12}C^{16}O_2$: 4550–7000 cm^{-1}. J Mol Spectrosc 2006;239:221–42.

[16] Perevalov BV, Campargue A, Gao B, Kassi S, Tashkun SA, Perevalov VI. New CW-CRDS measurements and global modeling of $^{12}C^{16}O_2$ absolute line intensities in the 1.6 μm region. J Mol Spectrosc 2008;252:190–7.

[17] Campargue A, Bailly D, Teffo JL, Tashkun SA, Perevalov VI. The v_1+5v_3 dyad of $^{12}CO_2$ and $^{13}CO_2$. J Mol Spectrosc 1999;193:204–12.

[18] Pollack JB, Dalton JB, Grinspoon D, Wattson RB, Freedman R, Crisp D, et al. Near-infrared light from venus nightside: a spectroscopic analysis. Icarus 1993;103:1–42.